HHS Public Access

Author manuscript

Cell Rep. Author manuscript; available in PMC 2021 June 23.

Published in final edited form as:

Cell Rep. 2021 June 01; 35(9): 109210. doi:10.1016/j.celrep.2021.109210.

Lactate dehydrogenase A-dependent aerobic glycolysis promotes natural killer cell anti-viral and anti-tumor function

Sam Sheppard[1], **Endi K. Santosa**[1,2], **Colleen M. Lau**[1], **Sara Violante**[3], **Paolo Giovanelli**[1,2], **Hyunu Kim**[1], **Justin R. Cross**[3], **Ming O. Li**[1,2], **Joseph C. Sun**[1,2,4,*]

[1]Immunology Program, Memorial Sloan Kettering Cancer Center, New York, NY 10065, USA

[2]Immunology and Microbial Pathogenesis Program, Graduate School of Medical Sciences, Weill Cornell Medical College, New York, NY 10065, USA

[3]Donald B. and Catherine C. Marron Cancer Metabolism Center, Memorial Sloan Kettering Cancer Center, New York, NY 10065, USA

[4]Lead contact

SUMMARY

Natural killer (NK) cells are cytotoxic lymphocytes capable of rapid cytotoxicity, cytokine secretion, and clonal expansion. To sustain such energetically demanding processes, NK cells must increase their metabolic capacity upon activation. However, little is known about the metabolic requirements specific to NK cells *in vivo*. To gain greater insight, we investigated the role of aerobic glycolysis in NK cell function and demonstrate that their glycolytic rate increases rapidly following viral infection and inflammation, prior to that of $CD8^+$ T cells. NK cell-specific deletion of lactate dehydrogenase A (LDHA) reveals that activated NK cells rely on this enzyme for both effector function and clonal proliferation, with the latter being shared with T cells. As a result, LDHA-deficient NK cells are defective in their anti-viral and anti-tumor protection. These findings suggest that aerobic glycolysis is a hallmark of NK cell activation that is key to their function.

In brief

Sheppard et al. demonstrate that lactate dehydrogenase A (LDHA)-mediated aerobic glycolysis is a hallmark of NK cell activation. LDHA-deficient NK cells, which are unable to perform aerobic glycolysis, are defective in their anti-viral and anti-tumor protection.

*Correspondence: sunj@mskcc.org.

AUTHOR CONTRIBUTIONS

S.S. and J.C.S. designed the study. S.S., P.G., and H.K. performed the experiments. S.V. and J.R.C. assisted with metabolic assays. M.O.L. provided mice critical to this study. E.K.S. and C.M.L. performed the bioinformatics analyses. S.S. and J.C.S. wrote the manuscript.

SUPPLEMENTAL INFORMATION

Supplemental information can be found online at https://doi.org/10.1016/j.celrep.2021.109210.

DECLARATION OF INTERESTS

The authors declare no competing interests.

Graphical abstract

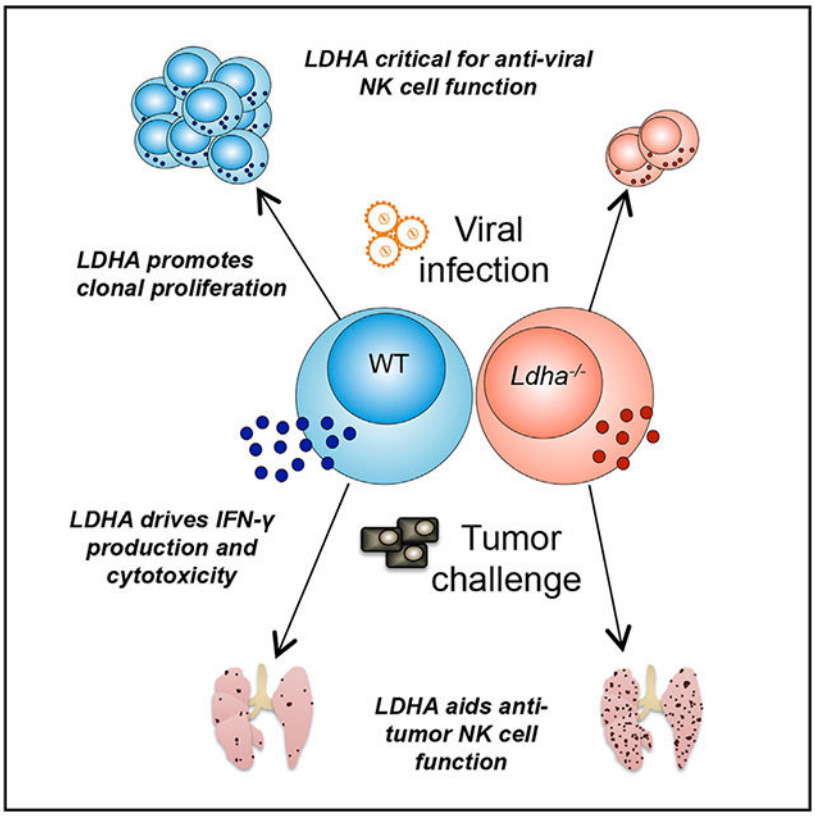

INTRODUCTION

During their activation, natural killer (NK) cells require metabolic reprogramming in order to support cytokine production and rapid proliferation (O'Brien and Finlay, 2019). *In vitro* metabolic studies of mouse and human NK cells have demonstrated that exposure to proinflammatory cytokines (e.g., interleukin [IL]-2, IL-12, and IL-15) increases both oxidative phosphorylation and glycolysis (Keating et al., 2016; Keppel et al., 2015; Marçais et al., 2014). These findings suggest that upregulation of metabolic pathways is one of the mechanisms by which cytokines activate NK cells. Key metabolic regulators that cytokines have been shown to activate include mTOR (Donnelly et al., 2014; Keating et al., 2016; Marçais et al., 2014) and MYC (Dong et al., 2019; Loftus et al., 2018). During *in vivo* immune challenges, NK cells are exposed to inflammatory cytokines and activating receptor stimuli; however, the changes these signals induce in the metabolic profile of NK cells are poorly characterized. Furthermore, although NK cells undoubtedly have metabolic demands that must be met for optimal activation, the precise metabolic pathways that are essential during *in vivo* immune challenges are also not well understood.

Blocking glucose metabolism using 2-deoxy-D-glucose (2-DG), a competitive inhibitor of glucose-6-phosphate production, or through culture in glucose-free media has suggested this pathway to be critical to optimal NK cell-activating receptor-induced interferon (IFN)-γ

production (Keppel et al., 2015) and control of mouse cytomegalovirus (MCMV) (Mah et al., 2017) *in vitro* and *in vivo*, respectively. However, because of potential pleiotropic and off-target effects of 2-DG *in vivo*, it is currently unknown which aspects of glucose metabolism are critical to NK cell function. Because glycolysis produces both ATP and substrates for biosynthetic pathways (e.g., nucleotide production) (Lane and Fan, 2015), we investigated the dependence of NK cell functional responses on aerobic glycolysis using a NK cell-specific genetic ablation of lactate dehydrogenase A (LDHA), as well as *in vivo* models of viral infection and tumor challenge. The conversion of pyruvate to lactate by LDHA helps maintain nicotinamide adenine dinucleotide (NAD^+) levels in the cell, sustaining glycolysis and the pentose phosphate pathways (PPPs). A better understanding of the role glycolytic regulation plays in NK cell functional responses will allow us to identify disease states where limited glycolysis is the barrier to optimal NK cell function, and aid in the development of NK cell-based therapies.

RESULTS AND DISCUSSION

NK cells rapidly induce glycolysis as part of their response to MCMV infection

During MCMV infection, NK cells mount a robust effector response, with $Ly49H^+$ cells undergoing clonal expansion and generating long-lived memory (Sun and Lanier, 2011). Thus, MCMV provides an excellent well-defined model in which to study the metabolic pathways regulating anti-viral NK cell effector functions. To investigate the metabolic changes occurring in NK cells after viral infection, we performed metabolite profiling using liquid chromatography-mass spectrometry on NK cells from the spleens of naive and infected mice. Analysis of more than 100 metabolites revealed that the levels of many glycolytic and pentose phosphate pathway intermediates are increased in NK cells within the first two days of MCMV infection (Figures 1A, 1B, and S1A). Phosphofructokinase uses ATP to convert fructose 6-phosphate to fructose 1,6-bisphosphate (FBP) and is the most important regulator of glycolytic flux (Sola-Penna et al., 2010). This process is inhibited by high concentrations of ATP and citrate, allowing it to react to the energy charge of a cell (Usenik and Legiša, 2010). In activated NK cells, we observed increased levels of FBP, which, in addition to dihydroxyacetone phosphate (DAP) (Figure 1A), have been shown to correlate with a higher rate of glycolysis (Tanner et al., 2018). Thus, we measured the glycolytic rate of naive and MCMV-activated $Ly49H^+$ NK cells *ex vivo* by assessing their extracellular acidification rate (ECAR) as a proxy for lactic acid production rate (Wu et al., 2007).We found that the ECAR of $Ly49H^+$ NK cells dramatically increases following MCMV infection, peaking at day 2 post-infection (PI) before returning to baseline in day 7 PI effector cells and day 30+ PI memory cells (Figure 1C). From the same MCMV-infected mice, we compared naive (day 0) and activated bulk (day 4 PI) or virus-specific (anti-M45 day 7 PI and day 30+ PI) $CD8^+$ T cells. In contrast to NK cells, as well as data from transgenic OT-1 T cells in *Listeria monocytogenes*-ovalbumin (OVA) infection, where the ECAR peaked at day 3 PI (Ma et al., 2019), the ECAR does not peak until day 7 PI in endogenous MCMV-reactive $CD8^+$ T cells; however, the maximum glycolytic rate reached similar levels to that of NK cells (Figures 1C and 1D). Thus, activation by viral infection *in vivo* rapidly increases the rate of aerobic glycolysis in NK cells prior to $CD8^+$ T cells. These observations agree with the widely accepted function of NK cells as the innate counterpart

of the $CD8^+$ T cell, able to rapidly respond while providing time for the adaptive immune responses to develop.

To better understand what drives the early increase in the glycolytic rate of NK cells during MCMV infection, we utilized transcriptional profiling of anti-viral NK cells (Lau et al., 2018) to examine which glycolytic pathway genes are differentially regulated in activated compared to naive NK cells. Using Kyoto Encyclopedia of Genes and Genomes (KEGG) pathway analysis at day 2 PI, we observed that many genes required for glycolysis and gluconeogenesis were transcriptionally upregulated compared to day 0 (Figure 1E). Among the upregulated genes were the glycolytic rate-limiting enzyme hexokinase (*Hk2*) and the enzyme key to aerobic glycolysis LDHA (*Ldha*) (Peng et al., 2016; Tanner et al., 2018). Expression of *Ldha* transcripts in NK cells during the course of MCMV infection showed the same pattern as their ECAR, with a rapid increase to peak *Ldha* expression at day 2 PI before returning to basal levels by days 7 and 30+ PI (Figures 1C and 1F).

T cells have been shown to rapidly upregulate aerobic glycolysis in response to T cell receptor (TCR) and coreceptor ligation (Frauwirth et al., 2002; Menk et al., 2018; Xu et al., 2021). Although early NK cell responses to MCMV infection are dependent on activation of pro-inflammatory cytokines (e.g., IL-12, IL-18, and type I IFNs; Madera and Sun, 2015; Sun et al., 2012), NK cells can also sense MCMV-infected cells via ligation of their activating receptor Ly49H to the virally encoded glycoprotein m157 (Arase et al., 2002; Brown et al., 2001; Daniels et al., 2001; Smith et al., 2002; Sun et al., 2009). Because the ECAR and transcriptomic data were generated using antigen-specific $Ly49H^+$ NK cells, the question remained whether induction of *Ldha* expression in NK cells was dependent on receptor ligation in addition to the inflammatory environment *in vivo*. Interestingly, we observed similar *Ldha* upregulation in $Ly49H^-$ NK cells after MCMV infection (Figure 1G), and *Ldha* mRNA was upregulated in NK cells following *in vitro* stimulation in the absence of Ly49H signaling with a cocktail of proinflammatory cytokines (IL-2 + IL-12 + IL +15 + IL-18) known to be produced during MCMV infection (Figure 1H). Taken together, these findings suggest that stimulation through proinflammatory cytokines alone can promote increases in the glycolytic capacity of NK cells. Thus, during viral infection, the glycolytic rate of NK cells is upregulated by the initial cytokine surge, but then returns to basal levels after 7 days, whereas glycolysis in anti-viral $CD8^+$ T cells peaks later, likely due to control of *Ldha* expression by TCR ligation rather than cytokines (Xu et al., 2021).

LDHA is not essential for NK cell development and homeostasis

LDHA converts pyruvate to L-lactate, and in doing so converts reduced NAD (NADH) into NAD^+, thus maintaining the supply of NAD^+ required to sustain rapid rates of glycolysis. As such, inhibition or ablation of LDHA can prevent cells from performing aerobic glycolysis (Oshima et al., 2020; Peng et al., 2016). To investigate whether aerobic glycolysis is essential for NK cell development, homeostasis, or anti-viral function *in vivo*, we generated mice with a NK cell-specific deletion of LDHA ($Ncr1^{Cre} \times Ldha^{flox/flox}$ mice, hereafter designated as NK cell-$Ldha^{-/-}$). As expected, when cultured with IL-15, LDHA-deficient NK cells produced significantly less lactate and consumed less glucose *in vitro* (Figures S2A and S2B). However, LDHA-deficient NK cells did not demonstrate significant differences in

development, with similar numbers of NK cells in the spleens of NK cell-*Ldha*$^{-/-}$ mice and their littermate wild-type (WT) control mice (Figure S2C). Expression of the receptors KLRG1, NKG2A/C/E, Ly49G2, Ly49H, and Ly49I were also similar in LDHA-deficient NK cells when compared to NK cells from littermate controls (Figure S2D). The proportion of mature NK cells, as defined by the loss of CD27 and gain of CD11b, was also similar between the two groups (Figure S2E–S2G). Next, we compared the basal ECAR and oxygen consumption rate (OCR) of LDHA-deficient NK cells to those of WT counterparts from mixed bone marrow chimeras. The basal ECAR and OCR of WT and LDHA-deficient NK cells were similar (Figure S2H), suggesting that aerobic glycolysis is not required for the development and maintenance of naive NK cells.

LDHA-mediated induction of aerobic glycolysis is essential for optimal anti-viral NK cell function

Because we did not observe any NK cell defects in the absence of LDHA at steady state, we investigated the importance of aerobic glycolysis during the response against MCMV infection. First, we measured the ECAR of *ex vivo* NK cells at day 2 PI. We observed a significant reduction in basal ECAR in LDHA-deficient NK cells (Figure 2A), suggesting that LDHA is driving aerobic glycolysis in anti-viral NK cells. This phenotype became even more pronounced after the addition of oligomycin (which prevents ATP synthesis, hyperpolarizes the mitochondria, and blocks the tricarboxylic acid [TCA] cycle), upon which the WT NK cells further increase their ECAR to compensate for the inhibition of oxidative phosphorylation while the LDHA-deficient NK cells failed to do so (Figure 2A). Comparison of oxidative respiration between WT and LDHA-deficient NK cells through measurement of OCR revealed a lack of difference (Figure 2A), suggesting that LDHA supports the production of critical biochemical substrates and/or maintenance of NAD^+, as opposed to the generation of ATP. Our data also suggests that LDHA deficiency prevents anti-viral NK cells from increasing their capacity to perform aerobic glycolysis.

To determine the functional importance of aerobic glycolysis induction in NK cells during MCMV infection, we challenged NK cell-*Ldha*$^{-/-}$ mice and their WT littermates with a high dose of virus. NK cell-*Ldha*$^{-/-}$ mice more rapidly succumbed to MCMV infection compared to WT controls (Figure 2B), suggesting that the induction of aerobic glycolysis in NK cells is vital for an effective anti-viral host immune response *in vivo*.

To better understand the impact of LDHA deletion in activated NK cells, we sorted and performed transcriptome analysis on WT and LDHA-deficient NK cells at steady state and following MCMV infection. Principal-component analysis (PCA) showed little variance between naive WT and LDHA-deficient NK cells (Figure 2C), corroborating our findings that LDHA ablation did not impact NK cell maturation or homeostasis (Figures S2C–S2G). However, the transcriptome of LDHA-deficient NK cells was clearly distinct from that of WT NK cells at day 2 PI (Figure 2C), with 2,580 genes differentially expressed (adjusted p $[p_{adj}] < 0.05$) between WT and LDHA-deficient NK cells on day 2 PI (Figure 2D). Analysis of genes differentially expressed on day 2 PI highlighted several pathways that were affected by the absence of LDHA, including the p53 and Ras pathways, as well as oxidative stress responses (Figure 2E). Genes regulating metabolism (*Hif1a, Mtor*, and *Vhl*), NK receptor

and cytokine signaling (*Zap70, Stat5b*, and *Mapk8/9*), and cellular proliferation (*Rras, Kras*, and *Cdk9/19*) were prominent among dysregulated pathways (Figure 2E). Thus, the activity of LDHA may be required for many aspects of anti-viral NK cell function.

LDHA is critical for NK cell clonal proliferation during MCMV infection

Given that many genes involved in cell survival and proliferation are dysregulated in LDHA-deficient NK cells during MCMV infection, we investigated the impact of LDHA deletion on anti-viral NK cell expansion. To do this, we transferred an equal number of NK cells from congenically distinct WT and NK cell-$Ldha^{-/-}$ mice into Ly49H-deficient hosts and infected them with MCMV. In this system, only adoptively transferred NK cells that express Ly49H are capable of antigen-specific clonal proliferation and memory formation in response to MCMV infection (Sun et al., 2009). We observed that the WT NK cells responded robustly to MCMV infection by rapidly expanding; however, the co-transferred LDHA-deficient NK cells were unable to mount an effective response and were quickly outcompeted by the WT cells at day 7 PI and beyond (Figures 3A and S3A). Furthermore, LDHA-deficient Ly49H$^+$ NK cells in spleen and liver showed diminished percentages of memory cells compared to WT controls (Figures 3B and S3B). Interestingly, LDHA-deficient Ly49H$^+$ NK cells showed a reduced expression level of Ly49H compared to WT Ly49H$^+$ NK cells at day 7 PI (Figure 3C), suggesting that LDHA is also required for the recently described avidity selection of NK cells (Adams et al., 2019; Grassmann et al., 2019). To confirm that the difference in effector and memory cell expansion was due to a proliferative defect, we labeled the NK cell populations with CellTrace Violet (CTV) priorto transfer and MCMV infection. By day 3.5 PI, a clear defect in the proliferative rate (measured by CTV dilution) of LDHA-deficient NK cells was observed when compared to their WT counterparts (Figure 3D). We also demonstrated that LDHA is critical for cytokine-driven proliferation *in vitro*, where cocultured WT but not LDHA-deficient NK cells underwent a significant expansion (Figure 3E). Thus, our data highlight an essential role for LDHA in the proliferative expansion of Ly49H$^+$ NK cells and host protection during MCMV infection, suggesting that the rapid upregulation of glycolytic metabolism is required for an effective NK cell-mediated anti-viral response.

We next investigated whether LDHA-dependent aerobic glycolysis was a shared requirement for clonal expansion between NK cells and T cells responding to virus infection. LDHA-deficient CD4$^+$ T cells had been previously shown to proliferate normally *in vitro* after stimulation with anti-CD3 and anti-CD28 in the presence of IL-2 (Peng et al., 2016). However, when we measured the proportion of CD8$^+$ T cells specific for MCMV epitopes derived from M45 and M38, representing canonical and inflationary T cell responses (Munks et al., 2006), respectively, we observed a higher prevalence of virus-specific CD8$^+$ T cells in the peripheral blood of WT mice compared to littermates with LDHA-deficient T cells (CD4^{Cre} × $Ldha^{flox/flox}$ mice, hereafter designated as T cell-$Ldha^{-/-}$) at all time points during MCMV infection (Figure 3F). These findings were corroborated with mixed bone marrow chimeric mice, where WT memory CD8$^+$ T cells were found in greater abundance than LDHA-deficient counterparts in both spleen and liver >30 days PI (Figure 3G). Thus, CD8$^+$ T cells require LDHA to mount a robust effector and memory response against viral

infection similar to Ly49H$^+$ NK cells, suggesting an important shared role for aerobic glycolysis in driving both innate and adaptive cytotoxic lymphocyte responses.

LDHA is required for optimal anti-tumor NK cell effector function

In addition to LDHA expression being important for driving proliferation, our transcriptional analysis of WT versus LDHA-deficient NK cells following MCMV infection also uncovered genes involved in NK cell activation (Figure 2E). To investigate the functional relevance of this finding, we stimulated naive NK cells from NK cell-*Ldha*$^{-/-}$ mice and their WT littermates with multiple concentrations of IL-12 + IL-18 *in vitro* and observed a similar proportion of cells producing IFN-γ between the two groups (Figure 4A). WT and LDHA-deficient NK cells similarly produced comparable levels of IFN-γ and granzyme B early after MCMV infection (Figure 4B). Thus, LDHA appears dispensable for cytokine-induced production of IFN-γ by NK cells. In contrast, following *in vitro* stimulation with phorbol 12-myristate 13-acetate (PMA) + ionomycin, a significantly reduced fraction of LDHA-deficient NK cells produced IFN-γ compared to WT controls (Figure 4C). Because ionomycin induces Ca^{2+} release from the endoplasmic reticulum (ER), which synergizes with PMA to activate calcium-sensitive kinases that are part of activating receptor signaling cascades (Chatila et al., 1989; Matthews and Cantrell, 2009), crosslinking of the NK cell-activating receptor NK1.1 also resulted in lower IFN-γ production in LDHA-deficient NK cells (Figure 4D).

We therefore tested whether LDHA deficiency had an impact on the cytotoxic function of NK cells by incubating calcein acetoxymethyl (calcein-AM)-labeled Yac-1 cells with NK cells isolated from either NK cell-*Ldha*$^{-/-}$ mice or their WT littermates. We observed a reduced lysis of Yac-1 cells by the LDHA-deficient NK cells (Figure 4E). Next, to dissect the importance of LDHA expression in NK cells participating in both “missing self”-induced and activating receptor-induced cytotoxic responses *in vivo*, we injected splenocytes from β_2-microglobulin β2m) knockout (KO) (major histocompatibility complex [MHC] class I-deficient) or m157 (Ly49H ligand) transgenic mice, respectively. Compared with labeled and co-injected WT control splenocytes, m157 transgenic or β2m KO splenocytes were less efficiently killed in NK cell-*Ldha*$^{-/-}$ mice compared to their WT littermates (Figures 4F and 4G). Altogether, these *in vitro* and *in vivo* data suggest that LDHA expression in NK cells is important for both activating receptor- and missing self-driven cytotoxicity.

Finally, we tested whether LDHA is vital for NK cell-mediated tumor surveillance *in vivo*. Using the NK cell-sensitive B16-F10 melanoma model of tumor metastasis, we challenged NK cell-*Ldha*$^{-/-}$ mice and their WT littermates and measured tumor burden 14 days later. The number of tumor nodules in the lung was significantly higher in NK cell-*Ldha*$^{-/-}$ mice compared to their WT littermates, suggesting that aerobic glycolysis is not only essential for optimal anti-viral but also anti-tumor function of NK cells (Figure 4H). Our results support recent findings that LDHA deficiency reduced the efficacy of CD8$^+$ T cells transferred as a therapeutic treatment into B16 tumor-bearing mice (Hermans et al., 2020).

In this study, we directly assess the glycolytic rate of NK cells *ex vivo* from virally infected mice. Previous *in vitro* studies of the metabolic regulation of NK cells have rapidly advanced

our understanding of lymphocyte metabolism. However, artificial levels of metabolite availability in a tissue culture dish can produce misleading results (Ma et al., 2019), and blockade of metabolic pathways with synthetic inhibitors such as 2-DG can have potential off-target side effects (Andresen et al., 2012; Kurtoglu et al., 2007; Zhong et al., 2008). Furthermore, use of inhibitors *in vivo* would likely target more than just NK cells, and pleiotropic effects would complicate interpretation of any phenotypes. In the present study, we engineered a NK cell-specific deletion of LDHA to investigate the role of aerobic glycolysis in the NK cell response against virus infection and tumor challenge. We discovered that during viral infection, NK cells rapidly induce aerobic glycolysis to levels similar to antigen-specific $CD8^+$ T cells, but with greater kinetics. Inhibition of aerobic glycolysis through cell-specific deletion of *Ldha* prevented NK cells and $CD8^+$ T cells from mounting a robust effector and memory response against MCMV infection.

Genetic ablation of LDHA prevents the inter-conversion of pyruvate to lactate. The prevailing view has been that LDHA converts pyruvate to lactate in rapidly dividing immune cells (Pearce et al., 2013) and that lactic acid inhibits the effector function of NK cells and T cells (Brand et al., 2016; Dodard et al., 2020; Fischer et al., 2007; Haas et al., 2015; Husain et al., 2013; Mendler et al., 2012). However, recent *in vivo* tracing studies have questioned these assertions. Mice infused with ^{13}C-lactate demonstrated significant lactate uptake by the spleen (Hui et al., 2017). Furthermore, *ex vivo* ^{13}C-glucose tracing in $CD8^+$ T cells from *Listeria*-infected mice demonstrated a significantly lower rate of lactate production than *in vitro* cultured T cells (Ma et al., 2019). Future studies will be required to demonstrate that activated NK cells are not utilizing lactate as a fuel source.

Proliferation of anti-viral NK cells is reliant on both aerobic glycolysis and oxidative phosphorylation (Mah-Som et al., 2021, this issue of *Cell Reports* This suggests that metabolic fitness is a key regulator of NK cell proliferation during an antiviral response. How these metabolic pathways regulate proliferation requires further investigation. It could simply be that a reduced concentration of metabolites becomes a rate-limiting factor for the biosynthesis of components required for proliferation. However, metabolites might also directly influence proliferation, as FBP was recently shown to activate Ras (Peeters et al., 2017). Thus, should stimulated NK cells suffer a reduction in levels of FBP or other metabolites, this may reduce proliferative signals and therefore the rate of cell division, possibly to preserve the cells and avoid apoptosis due to a lack of nutrient availability. This would be in line with previous findings from our lab that preventing the buildup of metabolism-induced stress, in the form of dysfunctional mitochondria, is key to robust NK cell memory formation (O'Sullivan et al., 2015).

It has previously been suggested that glucose metabolism promotes the production of IFN-γ in response to activating receptor ligation (Keppel et al., 2015). In this study, we demonstrate that LDHA tunes the responsiveness of NK cells to activating receptor stimulation potentially through aerobic glycolysis. In agreement with this finding, deletion of COX10, a critical component of the mitochondrial electron transport chain, had no negative impact on NK cell IFN-γ production in response to NK1.1 cross-linking or *in vitro* killing of Yac-1 cells (see accompanying article by Mah-Som et al., 2021). Thus, glucose metabolism likely

promotes IFN-γ production and NK cell cytotoxicity through the glycolytic pathway rather than through oxidative phosphorylation.

Glycolysis has been suggested to regulate IFN-γ production in T cells at both the transcriptional and post-transcriptional levels. Transcriptionally, glycolysis has been shown to maintain the high levels of acetyl-coenzyme A required to enhance histone acetylation and RNA polymerase II (RNA pol II) recruitment to the *Ifng* locus (Peng et al., 2016). Post-transcriptionally, glycolysis has been shown to prevent binding of substrate-free glyceraldehyde-3-phosphate dehydrogenase (GAPDH) to the 3′ UTR of *Ifng* mRNA, thereby relieving inhibition of translation (Chang et al., 2013). In NK cells, however, IFN-γ production in response to cytokine stimulation remained normal in the absence of LDHA, suggesting that *Ifng* expression is not impaired by either of these mechanisms. Moreover, LDHA-deficient NK cells exhibit defects in cytotoxicity, suggesting that glycolysis more broadly regulates their effector processes, likely through other mechanisms. A potential candidate is the reduced expression of members of the Ras and p38 mitogen-activated protein kinase (MAPK) pathways highlighted by our RNA sequencing (RNA-seq) analysis. This would seem to be in line with data suggesting that NK cell-activating receptor- but not cytokine-induced production of IFN-γ is dependent on the IκB kinase (IKK) complex and TPL2 (*Map3k8*) signaling (Piersma et al., 2019). A better understanding of how specific metabolic fitness regulates NK cells will be essential toward optimizing NK cell therapies.

STAR★METHODS

RESOURCE AVAILABILITY

Lead contact—Further information and requests for resources and reagents should be directed to and will be fulfilled by the Lead Contact, Joseph Sun (sunj@mskcc.org).

Materials availability—This study did not generate new unique reagents.

Data and code availability—Data generated in this study have been deposited in the Gene Expression Omnibus (GEO accession number GSE149447). Previously generated data referenced in this study can be found in GEO using accession number GSE106138.

EXPERIMENTAL MODEL AND SUBJECT DETAILS

Mice—All mice used in this study were housed and bred under specific pathogen free conditions at Memorial Sloan Kettering Cancer Center, and handled in accordance with the guidelines of the Institutional Animal Care and Use Committee (IACUC). The following mouse strains on a C57BL/6 background were used in this study: C57BL/6 (CD45.2), B6.SJL (CD45.1), B6 CD45.1xCD45.2, $Ncr1^{Cre}$ (Narni-Mancinelli et al., 2011), $Ldha^{flox}$ (Peng et al., 2016), $Ncr1^{Cre}$ x $Ldha^{flox/flox}$, $CD4^{Cre}$ x $Ldha^{flox/flox}$, $Klra8^{-/-}$ (Ly49H-deficient) (Fodil-Cornu et al., 2008), β2 m KO and m157 transgenic (Tripathy et al., 2008). Experiments were conducted using age- and sex-matched mice in accordance with approved institutional protocols.

Mixed bone marrow chimeras and adoptive transfers—Wild-type (WT) host $CD45.1^+$ $CD45.2^+$ mice were lethally irradiated with 900 Gy and reconstituted with a 1:1

mixture of bone marrow cells from WT (CD45.1$^+$) and either *Ncr1*^{Cre} × *Ldha*$^{flox/flox}$, *CD4*^{Cre} × *Ldha*$^{flox/flox}$ (CD45.2$^+$) mice. Intraperitoneal injection of mixed bone marrow chimeric mice with 200 μg of anti-NK1.1 (clone PK136) ensured depletion of any residual donor or host mature NK cells.

Adoptive co-transfer studies were performed by intravenously injecting an equal number of Ly49H$^+$ NK cells from WT (CD45.1) and gene-deficient (CD45.2) mice, or from mixed bone marrow chimeras, into *Klra8*$^{-/-}$ recipients before infecting recipient mice with MCMV.

METHOD DETAILS

Viral infection—Mixed bone marrow chimeric mice, *Klra8*$^{-/-}$ mice in adoptive transfer experiments, and mice in survival experiments received 7.5×10^3, 7.5×10^2, or 4×10^4 plaque-forming units (PFU) of MCMV (salivary gland passaged Smith strain) by i.p. injection, respectively.

Isolation of lymphocytes—Spleens and liver were dissociated through a 100-μm strainer. Dissociated liver was resuspended in a 40% Percoll solution and centrifuged at 700 × g (with reduced break speed) for 12 min to separate lymphocytes from hepatocytes. To isolate bone marrow cells, femur and tibia were ground with mortar and pestle and the resulting solution was filtered through a 100-μm strainer. Red blood cells in spleen, liver, blood, and bone marrow were lysed using ACK lysis buffer. In experiments involving sorted cells, splenocytes were incubated with rat anti-mouse CD3ε and CD8α (except when CD8$^+$ T cells were required) along with Ly6G, CD4, CD19, and Ter-119 antibodies (Bio X Cell, clones 17A2, 2.43, 1A8, GK1.5, 1D3, and TER-119, respectively) followed by incubation with BioMag goat anti-rat IgG beads (QIAGEN) to remove Ab-bound cells without touching populations of interest.

Flow cytometry and cell sorting—Surface staining of single-cell suspensions from bone marrow and spleen was performed using fluorophore-conjugated antibodies in the presence of Purified Rat Anti-Mouse CD16/CD32 (BD Bioscience) to block non-specific Fc binding and Fixable Viability Dye eFluor 506 (eBioscience/Thermo Fisher Scientific). Intracellular staining was performed by fixing and permeabilizing cells with the BD Cytofix/Cytoperm Fixation and Permeabilization kit (BD Bioscience). The following antibodies were used for flow cytometry: CD3ε (17A2, Tonbo, #25-0032), CD8α (53-6.7, BioLegend, #100730), CD11b (M1/70, eBioscience/Thermo Fisher Scientific, #467108), CD27 (LG.7F9, eBioscience/Thermo Fisher Scientific, #465001) CD45.1 (A20, BioLegend, #110729), CD45.2 (104, BioLegend, #109821), CD49b (DX5, BioLegend, #108918), CD69 (H1.2F3, BioLegend, #104524), Granzyme B (GB11, Biolegend, #2114575), IFN-γ (XMG1.2, eBioscience/Thermo Fisher Scientific, #1834366), Klrg1 (2F1, eBioscience/Thermo Fisher Scientific, #1518768) Ly49G2 (4D11, eBioscience/Thermo Fisher Scientific, #763604), Ly49H (3D10, eBioscience/Thermo Fisher Scientific, #11-5886-81) Ly49I (YLI-90, BD Bioscience, #2534427), NK1.1 (PK136, Tonbo, #65-5941), NKG2A/C/E (20d5, BD Bioscience, #465305) and TCRβ (H57-597, BioLegend, #109220). MHC class I tetramers were generated by conjugating D^b/HGIRNASFI (M45) or K^b/SSPPMFRV (M38) monomers (NIH Tetramer Facility) to streptavidin-PE or streptavidin-APC (BioLegend,

#405204 and #405207, respectively). NK cell proliferation was analyzed by labeling cells with 5 μM CellTrace Violet (CTV, Thermo Fisher) according to manufacturer's protocol prior to transfer into mice.

Flow cytometry and cell sorting were performed on LSR II and Aria II cytometers (BD Biosciences), respectively. NK cell activation on d2 PI was confirmed by expression of CD69. Virus-specific $CD8^+$ T cells were sorted using M45 tetramer staining at d7 PI and d30+ PI. Cells were sorted into 100 μL of FBS for RNA sequencing and mass spectrometry, or 20% FBS, 1mM EDTA, 25 mM HEPES in PBS for Seahorse. Flow cytometry data were analyzed with FlowJo software (Tree Star).

***In vitro* NK cell functional assays—**For receptor crosslinking, purified antibodies against NK1.1 (PK136) or isotype control were dispensed into high-binding ELISA plates at the concentration of 25 ug/ml in PBS, and allowed to adhere overnight at 4°C. For stimulation with cytokines, 20 ng/ml IL-18 plus 10 ng/ml of IL12 were added to the media. For PMA and ionomycin, 10 ng/ml and 1 μg/ml, respectively were added to the media. For all *ex vivo* stimulation, 2×10^5 bead enriched NK cells were plated in RPMI, and Brefeldin A (10 μg/ml; Sigma) and Golgi-Stop (0.7 μl/10^6 cells; BD) were added 2 hours after the culture started. Cells were analyzed by flow cytometry at 5h post-stimulation.

***In vitro* killing assay—**Yac-1 cells at a concentration of 1×10^6 cells per ml in phenol red free complete RPMI were stained with calcein-acetoxymethyl (calcein-AM) dye at a concentration of 15 μM for 30 minutes at 37°C. Excess dye was washed off prior to incubation with NK cells at a 20:1 effector:target ratio (3×10^3 targets per well) total volume of 200 μL in phenol read free complete RPMI in a 96 well plate. A maximum lysis control was generated by adding 100 μL of 2% Triton X-100 instead of effector cells, spontaneous lysis controls were created by adding 100 μL of media in place of effector cells. Cells were incubated together for 4 h at 37°C. Following incubation, the top 100 μL of cell free media was carefully transferred to a flat bottomed white 96 well plate and calcein AM release was read in a plate reader set to an excitation of 485 nm ± 9 nm and an emission of 525 nm ± 15nm. A percentage lysis was calculated by subtracting spontaneous lysis from all values then assuming the maximum lysis to be 100% lysis (Neri et al., 2001).

***In vivo* killing assay—**25×10^6 β2 m KO or m157 transgenic splenocytes were labeled with CTV or CTB and WT control splenocytes were stained with the other. (Labels was alternated in target cells between experimental repeats to control for any effect of the different dyes). Splenocytes were injected i.v. and mice were bled 24 h (β2M) or 3h (m157 transgenic) later. Killing was measured relative to co-transferred WT control splenocytes.

B16 metastasis—For the tumor metastasis *in vivo*, 2×10^5 B16-F10 cells were injected i.v. and mice were euthanized 14 days later. Lungs were harvested, and metastatic plaques counted.

Cytokine stimulation and qPCR—Sorted NK cells were cultured in complete RPMI with 10% FBS, containing IL-2 (20 ng/mL) + IL-12 (20 ng/mL) + IL-15 (20 ng/mL) + IL-18 (10 ng/mL) at 37°C for 3 hours. RNA was isolated using the PicoPure RNA Isolation Kit

following the manufacturer's instructions (Thermo Fisher Scientific). RNA was reverse transcribed into cDNA with a High capacity cDNA RT kit (Thermo Fisher Scientific). Quantitative real time PCR was carried out using the TaqMan system (*Ldha* Mm01612132_g1, Applied Biosystems), and values were normalized to *Actb* (Mm02619580_g1, Applied Biosystems) expression.

Cell culture—Sorted NK cells were cultured in complete IMDM with 10% FBS containing IL-15 (50 ng/ml) at 1.25-2.5 × 10^5 NK cells per mL. Cell counts were performed using 123count eBeads (Thermo Fisher Scientific) on a flow cytometer. Media was clarified by centrifugation at 800 xg for 3 mins and analyzed on a YSI biochemistry analyzer (YSI).

Seahorse bioanalyzer—5 × 10^5 NK cells or $CD8^+$ T cells were plated in buffer-free, glucose-free media (Seahorse Biosciences/ Agilent Technologies) with glutamine (2 mM), sodium pyruvate (0.5 mM), and glucose (10mM) for OCR and ECAR measurements, which were made under basal conditions and following addition of oligomycin (1 μM), FCCP (1 μM), Rotenone (1 μM) and Antimycin A (1 μM) at indicated time points and recorded on a Seahorse XFe96. All compounds added during the Seahorse run are from Seahorse Biosciences/Agilent Technologies.

Liquid chromatography-tandem mass spectrometry (LC-MS/MS) sample preparation—Sorted NK cells were pelleted at 800 × g for 3 mins 4°C, supernatant was aspirated, and pellets were frozen in liquid nitrogen. The intracellular metabolites were extracted by adding 1 mL ice-cold 80% methanol directly to the cell pellet and incubated overnight at −80°C to aid protein precipitation. The following day, the methanol extracts were centrifuged at 20,000 × *g* for 20 min at 4°C and 900 μL of the supernatant was transferred to a new tube and evaporated to dryness in a vacuum concentrator (GeneVac). The samples were reconstituted in 40 μL of 97:3 water:methanol containing 10 mM tributylamine and 15 mM acetic acid (mobile phase A) and incubated on ice for 20 min, vortexing every 5 min to ensure adequate re-suspension. All samples underwent one final centrifugation step (20,000 × *g* for 20 min at 4°C) to remove any residual particulate.

LC-MS/MS analysis—The reconstituted samples were subjected to MS/MS acquisition using an Agilent 1290 Infinity LC system equipped with a quaternary pump, multisampler, and thermostatted column compartment coupled to an Agilent 6470 series triple quadrupole system using a dual Agilent Jet Stream source for sample introduction. Data were acquired in dynamic MRM mode using electrospray ionization (ESI) in negative ion mode. The capillary voltage was 2000 V, nebulizer gas pressure of 45 psi, drying gas temperature of 150°C and drying gas flow rate of 13 L/min. A volume of 5 μL of sample was injected on to an Agilent Zorbax RRHD Extend-C18 (1.8 μm, 2.1 × 150 mm) column operating at 35°C. The 24 min chromatographic gradient was performed using 10 mM tributylamine and 15 mM acetic acid in 97:3 water:methanol (mobile phase A) and 10 mM tributylamine and 15 mM acetic acid in methanol (mobile phase B), at a 0.25 mL/minute flow rate. At the end of the 24 min, the gradient included a backflush of the analytical column for 6 min with 99% acetonitrile at a 0.8 mL/min flow rate, followed by a 5 min re-equilibration step at 100% A (MassHunter Metabolomics dMRM Database and Method, Agilent Technologies).

Each batch included method blanks and pooled samples. The pooled samples were prepared by mixing 5 μL of each sample in the batch. This mixture was injected multiple times as a control for changes during the run. Four technical replicates of the pooled sample were injected at the start of the batch to condition the system, followed by samples in randomized order. Analysis of the pooled samples was used to monitor the reproducibility of the system and the stability of the run over time. Initial data analysis was performed using MassHunter Quantitative Analysis (v. B.09.00). Following quantitative analysis, the files were exported to Mass Profiler Professional (v. 15.0) software for differential metabolite analysis. Statistical analysis was performed by applying a t test between the d0 and d2 groups and Benjamini-Hochberg correction ($p < 0.05$).

Sample preparation for RNA-seq—We sorted 2–6 × 10^4 splenic NK cells from mixed bone marrow chimeras for RNA-sequencing at d0 and d2 PI. Ly49H$^+$ NK cells were defined asTCRβ$^-$NK1.1$^+$ DX5$^+$ Ly49H$^+$ on d0, and also CD69$^+$ on d2 PI, along with either CD45.1$^+$ (WT) or CD45.2$^+$ (KO). Each sample represents an individual mouse. RNA was isolated from sorted cell populations using the PicoPure RNA Isolation Kit following the manufacturer's instructions (Thermo Fisher Scientific). After RiboGreen quantification and quality control by Agilent BioAnalyzer, 2 ng total RNA with RNA integrity numbers ranging from 9.4 to 10 underwent amplification using the SMART-Seq v4 Ultra Low Input RNA Kit (Clonetech catalog # 63488), with 12 cycles of amplification. Subsequently, 10 ng of amplified cDNA was used to prepare libraries with the KAPA Hyper Prep Kit (Kapa Biosystems KK8504) using 8 cycles of PCR. Samples were barcoded and run on a HiSeq 4000 in a 50bp/50bp paired end run, using the HiSeq 3000/4000 SBS Kit (Illumina). An average of 34 million paired reads were generated per sample and the percent of mRNA bases per sample ranged from 59% to 71%.

RNA-seq analysis—RNA-seq analysis on Ly49H$^+$ NK cells harvested at various time points during MCMV infection has been previously described (Lau et al., 2018). For RNA-seq generated in this study, paired-end reads were trimmed for adaptors and removal of low-quality reads using Trimmomatic (v0.36) (Bolger et al., 2014). Transcript quantification was based on the mm10 UCSC Known Gene models and performed using the quasi-mapping-based mode of Salmon (v.0.13.1) (Patro et al., 2017) correcting for potential GC bias. Transcripts were summarized to gene level using tximport (v1.10.1) (Soneson et al., 2015). Differential analyses were executed with DE-Seq2 (v1.22.2) (Love et al., 2014) using the UCSC Known Gene models as reference annotations. Genes were considered differential if they showed a P value (padj) < 0.05, adjusted for multiple hypothesis correction. Principal component analysis was performed using $\log_2$ values calculated by the *rlog* function from the DESeq2 package.

For gene set analysis, metabolism gene sets were retrieved from KEGG (https://www.kegg.jp/kegg/) through the Bioconductor KEGGREST package with the following identifiers: mmu00010 - Glycolysis/Gluconeogenesis; mmu00190 - Oxidative phosphorylation; mmu01212 - Fatty acid metabolism). Gene set enrichment was performed on downregulated differentially expressed genes (LDHA-deficient versus WT) with goseq (v1.34.1) (Young et al., 2010), using pathways from the PANTHER database (http://

www.pantherdb.org/) retrieved through the Bioconductor Panther.db package. P values were corrected for multiple-hypothesis testing using the Benjamini & Hochberg method.

QUANTIFICATION AND STATISTICAL ANALYSIS

Statistical analyses—For graphs, data are shown as mean ± SD, and unless otherwise indicated, statistical differences were evaluated using a two-tailed unpaired Student's t test. Equal sample variance was assumed; unless an F test demonstrated significant variance then Welch's correction was applied. Statistical differences in survival were determined by log-rank (Mantel-Cox) Test analysis. $p < 0.05$ was considered significant. Graphs were produced and statistical analyses were performed using GraphPad Prism.

Supplementary Material

Refer to Web version on PubMed Central for supplementary material.

ACKNOWLEDGMENTS

We thank members of the Sun laboratory for comments, discussions, technical support, and experimental assistance. We thank Annelise Mah-Som and Megan Cooper for sharing their manuscript with us prior to publication. The NIH tetramer core generated monomers used in this study. C.M.L. was supported by the Cancer Research Institute as a Cancer Research Institute-Carson Family Fellow. We acknowledge the use of the Integrated Genomics Operation Core, funded by the NCI Cancer Center Support Grant (P30CA08748), Cycle for Survival, and the Marie-Josée and Henry R. Kravis Center for Molecular Oncology. J.R.C. was supported by the Tri-Institutional Metabolomics Training Program (R25AI140472). J.C.S. was supported by the Ludwig Center for Cancer Immunotherapy, the American Cancer Society, the Burroughs Wellcome Fund, and the NIH (AI100874, AI130043, and AI155558).

REFERENCES

Adams NM, Geary CD, Santosa EK, Lumaquin D, Le Luduec JB, Sottile R, van der Ploeg K, Hsu J, Whitlock BM, Jackson BT, et al.. (2019). Cytomegalovirus infection drives avidity selection of natural killer cells. Immunity 50, 1381–1390.e5. [PubMed: 31103381]

Andresen L, Skovbakke SL, Persson G, Hagemann-Jensen M, Hansen KA, Jensen H, and Skov S (2012). 2-Deoxy D-glucose prevents cell surface expression of NKG2D ligands through inhibition of N-linked glycosylation. J. Immunol 188, 1847–1855. [PubMed: 22227571]

Arase H, Mocarski ES, Campbell AE, Hill AB, and Lanier LL (2002). Direct recognition of cytomegalovirus by activating and inhibitory NK cell receptors. Science 296, 1323–1326. [PubMed: 11950999]

Bolger AM, Lohse M, and Usadel B (2014). Trimmomatic: A flexible trimmer for Illumina sequence data. Bioinformatics 30, 2114–2120. [PubMed: 24695404]

Brand A, Singer K, Koehl GE, Kolitzus M, Schoenhammer G, Thiel A, Matos C, Bruss C, Klobuch S, Peter K, et al.. (2016). LDHA-associated lactic acid production blunts tumor immunosurveillance by T and NK cells. Cell Metab. 24, 657–671. [PubMed: 27641098]

Brown MG, Dokun AO, Heusel JW, Smith HRC, Beckman DL, Blattenberger EA, Dubbelde CE, Stone LR, Scalzo AA, and Yokoyama WM (2001). Vital involvement of a natural killer cell activation receptor in resistance to viral infection. Science 292, 934–937. [PubMed: 11340207]

Chang CH, Curtis JD, Maggi LB Jr., Faubert B, Villarino AV, O'Sullivan D, Huang SCC, van der Windt GJW, Blagih J, Qiu J, et al. (2013). Posttranscriptional control of T cell effect or function by aerobic glycolysis. Cell 153, 1239–1251. [PubMed: 23746840]

Chatila T, Silverman L, Miller R, and Geha R (1989). Mechanisms of T cell activation by the calcium ionophore ionomycin. J. Immunol 143, 1283–1289. [PubMed: 2545785]

Daniels KA, Devora G, Lai WC, O'Donnell CL, Bennett M, and Welsh RM (2001). Murine cytomegalovirus is regulated by a discrete subset of natural killer cells reactive with monoclonal antibody to Ly49H. J. Exp. Med 194, 29–44. [PubMed: 11435470]

Dodard G, Tata A, Erick TK, Jaime D, Miah SMS, Quatrini L, Escalière B, Ugolini S, Vivier E, and Brossay L (2020). Inflammation-induced lactate leads to rapid loss of hepatic tissue-resident NK cells. Cell Rep 32, 107855. [PubMed: 32640221]

Dong H, Adams NM, Xu Y, Cao J, Allan DSJ, Carlyle JR, Chen X, Sun JC, and Glimcher LH (2019). The IRE1 endoplasmic reticulum stress sensor activates natural killer cell immunity in part by regulating c-Myc. Nat. Immunol 20, 865–878. [PubMed: 31086333]

Donnelly RP, Loftus RM, Keating SE, Liou KT, Biron CA, Gardiner CM, and Finlay DK (2014). mTORC1-dependent metabolic reprogramming is a prerequisite for NK cell effector function. J. Immunol 193, 4477–4484. [PubMed: 25261477]

Fischer K, Hoffmann P, Voelkl S, Meidenbauer N, Ammer J, Edinger M, Gottfried E, Schwarz S, Rothe G, Hoves S, et al. (2007). Inhibitory effect of tumor cell-derived lactic acid on human T cells. Blood 109, 3812–3819. [PubMed: 17255361]

Fodil-Cornu N, Lee S-H, Belanger S, Makrigiannis AP, Biron CA, Buller RM, and Vidal SM (2008). Ly49h-deficient C57BL/6 mice: A new mouse cytomegalovirus-susceptible model remains resistant to unrelated pathogens controlled by the NK gene complex. J. Immunol 181, 6394–6405. [PubMed: 18941230]

Frauwirth KA, Riley JL, Harris MH, Parry RV, Rathmell JC, Plas DR, Elstrom RL, June CH, and Thompson CB (2002). The CD28 signaling pathway regulates glucose metabolism. Immunity 16, 769–777. [PubMed: 12121659]

Grassmann S, Pachmayr LO, Leube J, Mihatsch L, Andrae I, Flommersfeld S, Oduro J, Cicin-Sain L, Schiemann M, Flossdorf M, and Buchholz VR (2019). Distinct surface expression of activating receptor Ly49H drives differential expansion of NK cell clones upon murine cytomegalovirus infection. Immunity 50, 1391–1400.e4. [PubMed: 31103380]

Haas R, Smith J, Rocher-Ros V, Nadkarni S, Montero-Melendez T, D'Acquisto F, Bland EJ, Bombardieri M, Pitzalis C, Perretti M, et al.. (2015). Lactate regulates metabolic and pro-inflammatory circuits in control of T cell migration and effector functions. PLoS Biol. 13, e1002202. [PubMed: 26181372]

Hermans D, Gautam S, García-Cañaveras JC, Gromer D, Mitra S, Spolski R, Li P, Christensen S, Nguyen R, Lin JX, et al.. (2020). Lactate dehydrogenase inhibition synergizes with IL-21 to promote $CD8^+$ T cell stemness and antitumor immunity. Proc. Natl. Acad. Sci. USA 117, 6047–6055. [PubMed: 32123114]

Hui S, Ghergurovich JM, Morscher RJ, Jang C, Teng X, Lu W, Esparza LA, Reya T, Le Zhan, Yanxiang Guo J, et al.. (2017). Glucose feeds the TCA cycle via circulating lactate. Nature 551, 115–118. [PubMed: 29045397]

Husain Z, Huang Y, Seth P, and Sukhatme VP (2013). Tumor-derived lactate modifies antitumor immune response: Effect on myeloid-derived suppressor cells and NK cells. J. Immunol 191, 1486–1495. [PubMed: 23817426]

Keating SE, Zaiatz-Bittencourt V, Loftus RM, Keane C, Brennan K, Finlay DK, and Gardiner CM (2016). Metabolic reprogramming supports IFN-γ production by $CD56^{bright}$ NK Cells. J. Immunol 196, 2552–2560. [PubMed: 26873994]

Keppel MP, Saucier N, Mah AY, Vogel TP, and Cooper MA (2015). Activation-specific metabolic requirements for NK cell IFN-γ production. J. Immunol 194, 1954–1962. [PubMed: 25595780]

Kurtoglu M, Maher JC, and Lampidis TJ (2007). Differential toxic mechanisms of 2-deoxy-D-glucose versus 2-fluorodeoxy-D-glucose in hypoxic and normoxic tumor cells. Antioxid. Redox Signal. 9, 1383–1390. [PubMed: 17627467]

Lane AN, and Fan TWM (2015). Regulation of mammalian nucleotide metabolism and biosynthesis. Nucleic Acids Res. 43, 2466–2485. [PubMed: 25628363]

Langmead B, and Salzberg S (2012). Fast gapped-read alignment with Bowtie 2. Nat Methods 9, 357–359. 10.1038/nmeth.1923. [PubMed: 22388286]

Lau CM, Adams NM, Geary CD, Weizman O-E, Rapp M, Pritykin Y, Leslie CS, and Sun JC (2018). Epigenetic control of innate and adaptive immune memory. Nat. Immunol 19, 963–972. [PubMed: 30082830]

Loftus RM, Assmann N, Kedia-Mehta N, O'Brien KL, Garcia A, Gillespie C, Hukelmann JL, Oefner PJ, Lamond AI, Gardiner CM, et al.. (2018). Amino acid-dependent cMyc expression is essential for NK cell metabolic and functional responses in mice. Nat. Commun 9, 2341. [PubMed: 29904050]

Love MI, Huber W, and Anders S (2014). Moderated estimation of fold change and dispersion for RNA-seq data with DESeq2. Genome Biol. 15, 550. [PubMed: 25516281]

Ma EH, Verway MJ, Johnson RM, Roy DG, Steadman M, Hayes S, Williams KS, Sheldon RD, Samborska B, Kosinski PA, et al.. (2019). Metabolic profiling using stable isotope tracing reveals distinct patterns of glucose utilization by physiologically activated $CD8^+$ T cells. Immunity 51, 856–870.e5. [PubMed: 31747582]

Madera S, and Sun JC (2015). Cutting edge: Stage-specific requirement of IL-18 for antiviral NK cell expansion. J. Immunol 194, 1408–1412. [PubMed: 25589075]

Mah AY, Rashidi A, Keppel MP, Saucier N, Moore EK, Alinger JB, Tripathy SK, Agarwal SK, Jeng EK, Wong HC, et al.. (2017). Glycolytic requirement for NK cell cytotoxicity and cytomegalovirus control. JCI Insight 2, e95128.

Mah-Som AY, Keppel MP, Tobin JM, Kolicheski A, Saucier N, Sexl V, French AR, Wagner JA, Fehniger TA, and Cooper MA (2021). Reliance on Cox10 and oxidative metabolism for antigen-specific NK cell expansion. Cell Rep. 35, this issue, 109209-1–109209-11. [PubMed: 34077722]

Marçais A, Cherfils-Vicini J, Viant C, Degouve S, Viel S, Fenis A, Rabilloud J, Mayol K, Tavares A, Bienvenu J, et al.. (2014). The metabolic checkpoint kinase mTOR is essential for IL-15 signaling during NK cell development and activation of NK cells. Nat. Immunol 15, 749–757. [PubMed: 24973821]

Matthews SA, and Cantrell DA (2009). New insights into the regulation and function of serine/threonine kinases in T lymphocytes. Immunol. Rev 228, 241–252. [PubMed: 19290932]

Mendler AN, Hu B, Prinz PU, Kreutz M, Gottfried E, and Noessner E (2012). Tumor lactic acidosis suppresses CTL function by inhibition of p38 and JNK/c-Jun activation. Int. J. Cancer 131, 633–640. [PubMed: 21898391]

Menk AV, Scharping NE, Moreci RS, Zeng X, Guy C, Salvatore S, Bae H, Xie J, Young HA, Wendell SG, and Delgoffe GM (2018). Early TCR signaling induces rapid aerobic glycolysis enabling distinct acute T cell effector functions. Cell Rep. 22, 1509–1521. [PubMed: 29425506]

Munks MW, Cho KS, Pinto AK, Sierro S, Klenerman P, and Hill AB (2006). Four distinct patterns of memory CD8 T cell responses to chronic murine cytomegalovirus infection. J. Immunol 177, 450–458. [PubMed: 16785542]

Narni-Mancinelli E, Chaix J, Fenis A, Kerdiles YM, Yessaad N, Reynders A, Gregoire C, Luche H, Ugolini S, Tomasello E, et al.. (2011). Fate mapping analysis of lymphoid cells expressing the NKp46 cell surface receptor. Proc. Natl. Acad. Sci. USA 108, 18324–18329. [PubMed: 22021440]

Neri S, Mariani E, Meneghetti A, Cattini L, and Facchini A (2001). Calcein-acetyoxymethyl cytotoxicity assay: Standardization of a method allowing additional analyses on recovered effector cells and supernatants. Clin. Diagn. Lab. Immunol 8, 1131–1135. [PubMed: 11687452]

O'Brien KL, and Finlay DK (2019). Immunometabolism and natural killer cell responses. Nat. Rev. Immunol 19, 282–290. [PubMed: 30808985]

O'Sullivan TE, Johnson LR, Kang HH, and Sun JC (2015). BNIP3- and BNIP3L-mediated mitophagy promotes the generation of natural killer cell memory. Immunity 43, 331–342. [PubMed: 26253785]

Oshima N, Ishida R, Kishimoto S, Beebe K, Brender JR, Yamamoto K, Urban D, Rai G, Johnson MS, Benavides G, et al.. (2020). Dynamic imaging of LDH inhibition in tumors reveals rapid in vivo metabolic rewiring and vulnerability to combination therapy. Cell Rep. 30, 1798–1810.e4. [PubMed: 32049011]

Patro R, Duggal G, Love MI, Irizarry RA, and Kingsford C (2017). Salmon provides fast and bias-aware quantification of transcript expression. Nat. Methods 14, 417–419. [PubMed: 28263959]

Pearce EL, Poffenberger MC, Chang CH, and Jones RG (2013). Fueling immunity: Insights into metabolism and lymphocyte function. Science 342, 1242454. [PubMed: 24115444]

Peeters K, Van Leemputte F, Fischer B, Bonini BM, Quezada H, Tsytlonok M, Haesen D, Vanthienen W, Bernardes N, Gonzalez-Blas CB, et al.. (2017). Fructose-1,6-bisphosphate couples glycolytic flux to activation of Ras. Nat. Commun 8, 922. [PubMed: 29030545]

Peng M, Yin N, Chhangawala S, Xu K, Leslie CS, and Li MO (2016). Aerobic glycolysis promotes T helper 1 cell differentiation through an epigenetic mechanism. Science 354, 481–484. [PubMed: 27708054]

Piersma SJ, Pak-Wittel MA, Lin A, Plougastel-Douglas B, and Yokoyama WM (2019). Activation receptor-dependent IFN-γ production by NK cells is controlled by transcription, translation, and the proteasome. J. Immunol 203, 1981–1988. [PubMed: 31444264]

Smith HRC, Heusel JW, Mehta IK, Kim S, Dorner BG, Naidenko OV, Iizuka K, Furukawa H, Beckman DL, Pingel JT, et al.. (2002). Recognition of a virus-encoded ligand by a natural killer cell activation receptor. Proc. Natl. Acad. Sci. USA 99, 8826–8831. [PubMed: 12060703]

Sola-Penna M, DaSilva D, Coelho WS, Marinho-Carvalho MM,and Zancan P (2010). Regulation of mammalian muscle type 6-phosphofructo-1-kinase and its implication for the control of the metabolism. IUBMB Life 62, 791–796. [PubMed: 21117169]

Soneson C, Love MI, and Robinson MD (2015). Differential analyses for RNA-seq: transcript-level estimates improve gene-level inferences. F1000Res. 4, 1521. [PubMed: 26925227]

Sun JC, and Lanier LL (2011). NKcell development, homeostasis and function: Parallels with $CD8^+$ T cells. Nat. Rev. Immunol 11, 645–657. [PubMed: 21869816]

Sun JC, Beilke JN, and Lanier LL (2009). Adaptive immune features of natural killer cells. Nature 457, 557–561. [PubMed: 19136945]

Sun JC, Madera S, Bezman NA, Beilke JN, Kaplan MH, and Lanier LL (2012). Proinflammatory cytokine signaling required for the generation of natural killer cell memory. J. Exp. Med 209, 947–954. [PubMed: 22493516]

Tanner LB, Goglia AG, Wei MH, Sehgal T, Parsons LR, Park JO, White E, Toettcher JE, and Rabinowitz JD (2018). Four key steps control glycolytic flux in mammalian cells. Cell Syst. 7, 49–62.e8. [PubMed: 29960885]

Tripathy SK, Keyel PA, Yang L, Pingel JT, Cheng TP, Schneeberger A, and Yokoyama WM (2008). Continuous engagement of a self-specific activation receptor induces NK cell tolerance. J. Exp. Med 205, 1829–1841. [PubMed: 18606857]

Usenik A, and Legiša M (2010). Evolution of allosteric citrate binding sites on 6-phosphofructo-1-kinase. PLoS ONE 5, e15447. [PubMed: 21124851]

Wu M, Neilson A, Swift AL, Moran R, Tamagnine J, Parslow D, Armistead S, Lemire K, Orrell J, Teich J, et al.. (2007). Multiparameter metabolic analysis reveals a close link between attenuated mitochondrial bioenergetic function and enhanced glycolysis dependency in human tumor cells. Am. J. Physiol. Cell Physiol 292, C125–C136. [PubMed: 16971499]

Xu K, Yin N, Peng M, Stamatiades EG, Shyu A, Li P, Zhang X, Do MH, Wang Z, Capistrano KJ, et al.. (2021). Glycolysis fuels phosphoinositide 3-kinase signaling to bolster T cell immunity. Science 371, 405–410. [PubMed: 33479154]

Young MD, Wakefield MJ, Smyth GK, and Oshlack A (2010). Gene ontology analysis for RNA-seq: accounting for selection bias. Genome Biol. 11, R14. [PubMed: 20132535]

Zhong D, Liu X, Schafer-Hales K, Marcus AI, Khuri FR, Sun SY, and Zhou W (2008). 2-Deoxyglucose induces Akt phosphorylation via a mechanism independent of LKB1/AMP-activated protein kinase signaling activation or glycolysis inhibition. Mol. Cancer Ther 7, 809–817. [PubMed: 18413794]

Highlights

- During viral infection, inflammatory cytokines induce aerobic glycolysis in NK cells
- *Ldha* expression is critical for clonal expansion of host-protective anti-viral NK and $CD8^+$ T cells
- LDHA facilitates NK cell-activating receptor signaling and effector function
- NK cells rely on LDHA for their elimination of tumors

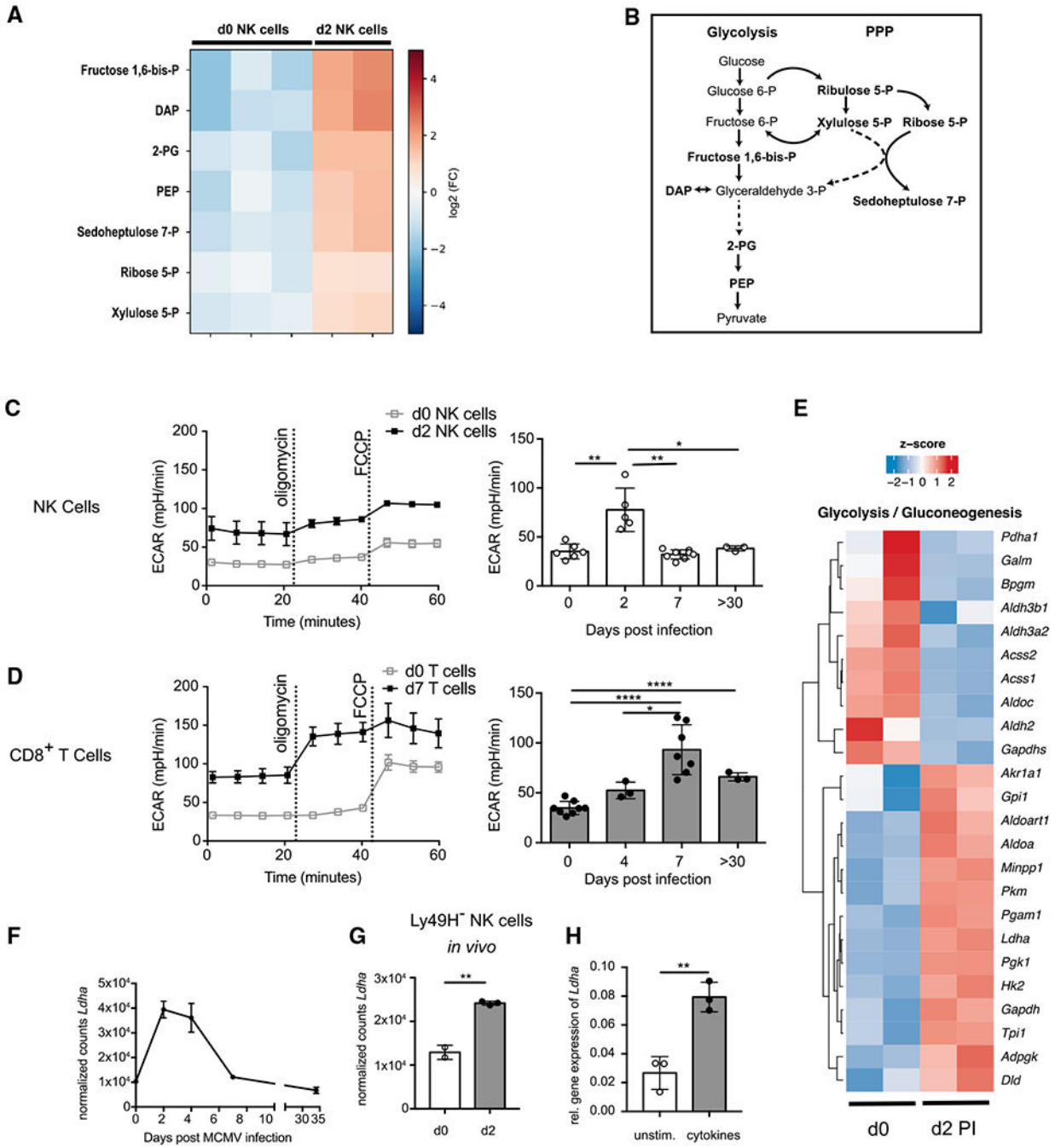

Figure 1. NK cells rapidly upregulate glycolysis during MCMV infection

(A and B) NK cells were harvested from naive and MCMV-infected mice at 2 days post-infection (PI), and mass spectrometry was used to assess metabolite relative abundance. (A) Glycolytic and pentose phosphate pathway metabolites that passed significance testing (unpaired t test, $p \leq 0.05$, fold change [FC] ≥ 2) between day 0 and day 2 PI are shown in the heatmap. Each sample represents an average of two technical replicates. Raw peak area counts for each metabolite were baselined to the mean of all samples prior to $\log_2$ transformation.

(B) Diagram of the glycolysis and pentose phosphate pathways; metabolites in bold are upregulated in NK cells on day 2 PI. P, phosphate; DAP, dihydroxyacetone phosphate; 2-PG, 2-phosphoglycerate; PEP, phosphoenolpyruvate.

(C and D) Representative and summary plots of the extracellular acidification rate(ECAR) of 5×10^5splenic Ly49H$^+$ NK cells (C) or CD8$^+$ T cells (D) *ex vivo*, pooled from naive (day 0) or MCMV-infected mice at indicated number of days following MCMV infection under basal conditions (in summary plots), and in response to indicated metabolic inhibitors.

(E) Heatmap of KEGG glycolysis/gluconeogenesis pathway gene expression measured by RNA-seq. Genes shown are those that are differentially expressed in splenic Ly49H$^+$ NK cells at day 0 versus day 2 PI. mRNA expression levels are row-scaled and log-transformed.

(F) Normalized counts of *Ldha* mRNA expression in Ly49H$^+$ NK cells at various time points during MCMV infection measured by RNA-seq.

(G) Normalized counts of *Ldha* mRNA expression measured by RNA-seq in Ly49H$^-$ NK cells from mice at day 0 and day 2 PI.

(H) Expression level of *Ldha* mRNA relative to *Actb* mRNA measured by qRT-PCR in purified splenic NK cells stimulated for 3 h with IL-2 + IL-12 + IL-15 + IL-18. Means are plotted ± SD. *p < 0.05, **p < 0.01, ****p < 0.0001 (Student's t test). Data are representative of two or more independent experiments; n = 2–8.

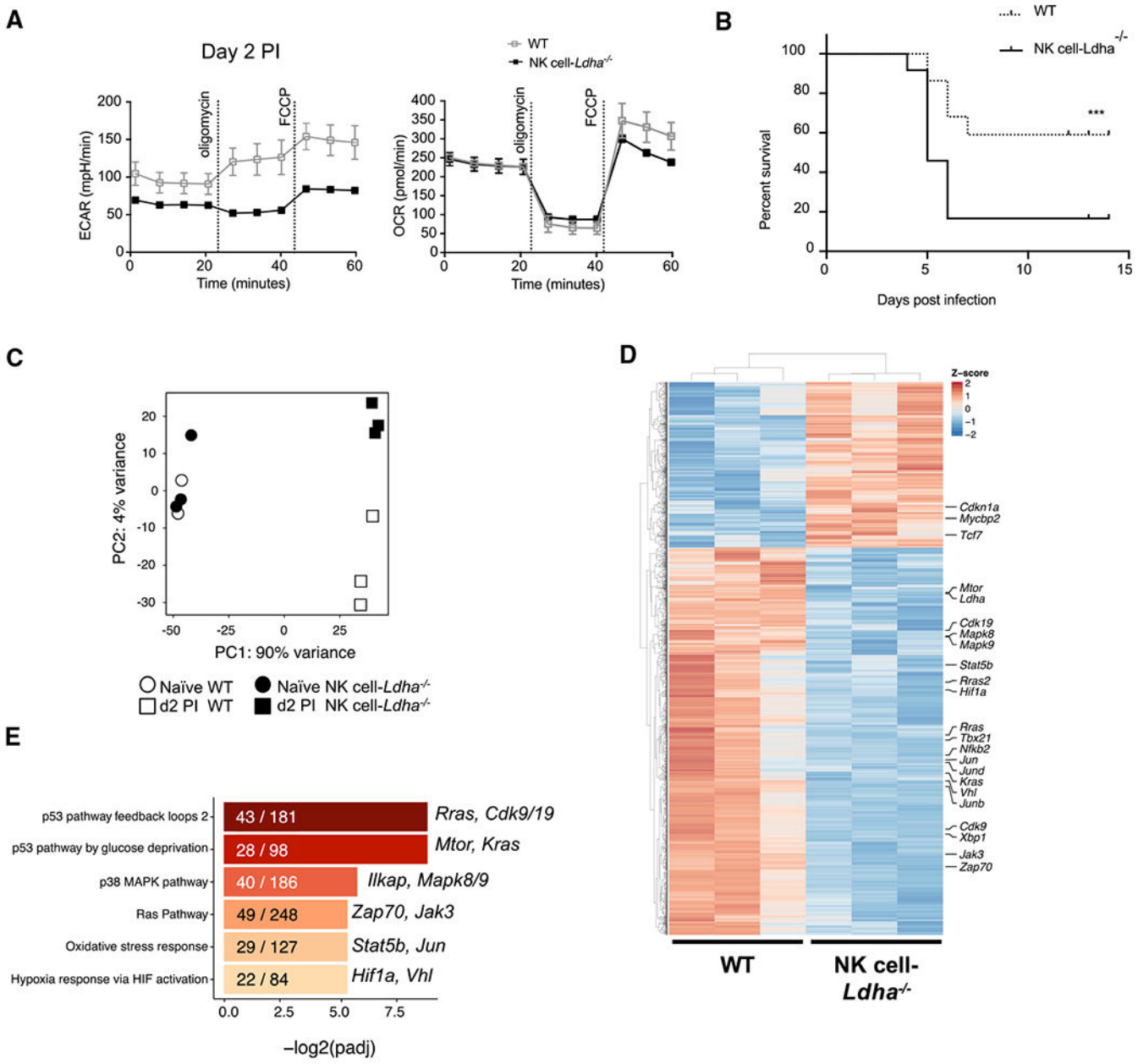

Figure 2. LDHA is essential for optimal anti-viral NK cell function

(A) Representative *ex vivo* ECAR of 5×10^5 splenic NK cells from mixed $Ncr1^{Cre} \times Ldha^{flox/flox}$ (CD45.2) and WT (CD45.1) bone marrow chimeric mice at day 2 PI. Means are plotted ± SD and are representative of three independent experiments. ***$p < 0.001$.

(B) Kaplan-Meier representation of the survival of mice containing LDHA-deficient NK cells ($Ncr1^{Cre} \times Ldha^{flox/flox}$) or WT NK cells ($Ldha^{flox/flox}$) following MCMV challenge, with significant differences determined by a log-rank test ($p = 0.0007$). Plot combines the results of three independent experiments.

(C–E) RNA-seq was generated from Ly49H$^+$ NK cells sorted from the spleens of mixed $Ncr1^{Cre} \times Ldha^{flox/flox}$ (CD45.2) and WT (CD45.1) bone marrow chimeric mice at day 0

versus day 2 PI (n = 3). (C) PCA of RNA-seq data, showing the impact of *Ldha* deletion on gene expression. (D) Heatmap of 2,878 genes differentially expressed in WT or LDHA-deficient NK cells at day 2 PI ($p_{adj} < 0.05$) and (E) pathways predicted to be impacted by the data in (D) defined using the PANTHER database.

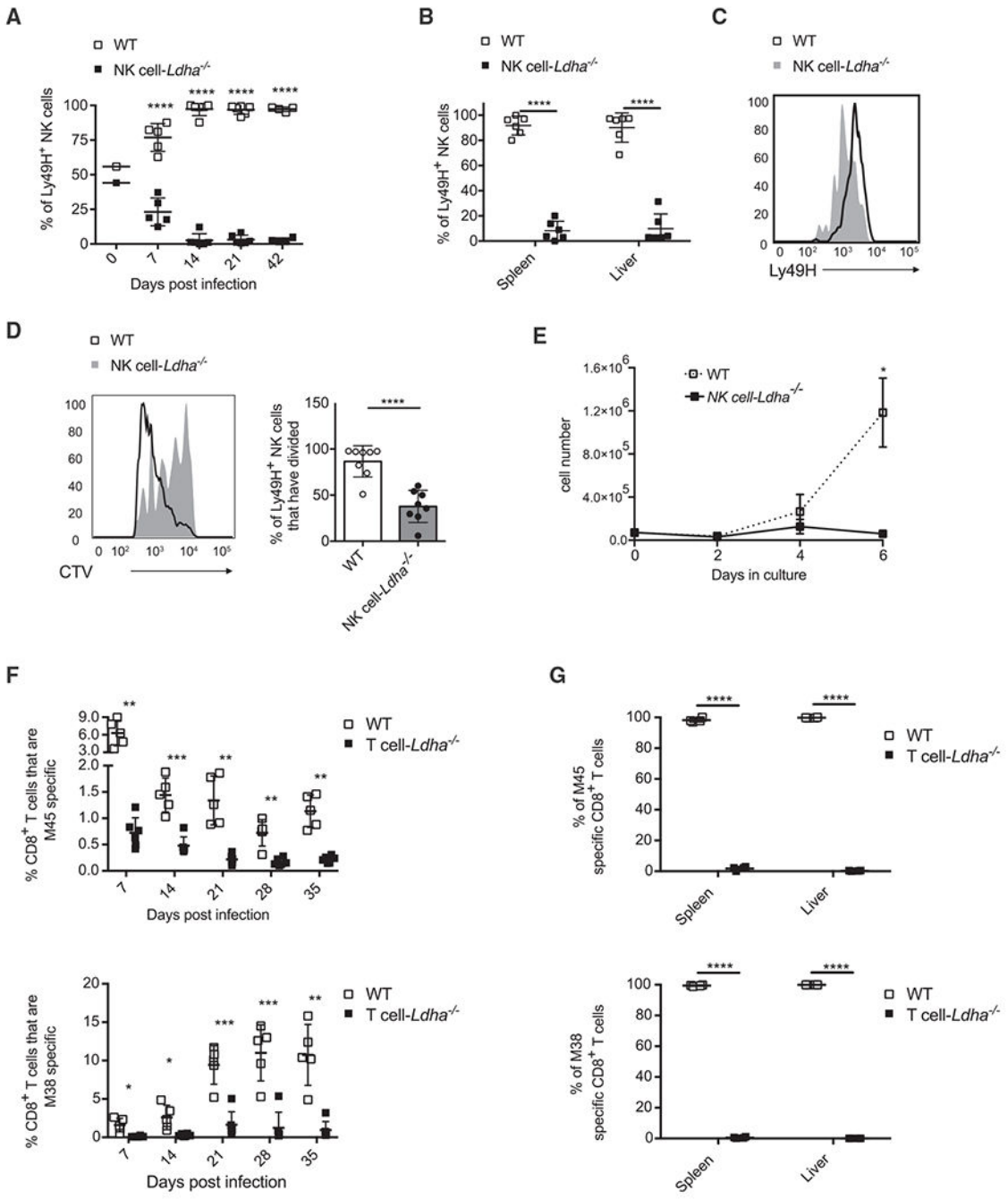

Figure 3. LDHA promotes NK and CD8$^+$ T cell proliferation in response to MCMV infection

(A and B) Percentage of transferred Ly49H$^+$ NK cells that are WT (CD45.1) versus *Ncr1*^{Cre} × *Ldha*$^{flox/flox}$ (CD45.2) in the blood of Ly49H-deficient hosts during the course of MCMV infection (A), and in the spleen and liver harvested at >30 days PI (B).

(C) Ly49H expression level of Ly49H$^+$ WT and LDHA-deficient NK cells at day 7 PI.

(D) Prior to transfer into Ly49H-deficient recipient mice, the two NK cell populations were labeled with CellTrace Violet (CTV). Mice were sacrificed 3.5days PI, and the representative flow plot and graph show cell division assessed by dilution of CTV.

(E) *Ex vivo* WT (CD45.1) and $Ncr1^{Cre} \times Ldha^{flox/flox}$ (CD45.2) NK cells were co-cultured in IL-15, and cell numbers were determined by flow cytometry at indicated time points.
(F) Percentage of M45- and M38-specific populations within total $CD8^+$ T cells from the peripheral blood of $CD4^{Cre} \times Ldha^{flox/flox}$ and $Ldha^{flox/flox}$ littermate controls (WT) at various time points following MCMV infection.
(G) Percentage of M45- and M38-specific memory $CD8^+$ T cells from $CD4^{Cre} \times Ldha^{flox/flox}$ (CD45.2) or WT (CD45.1) populations in the spleen and liver of mixed bone marrow chimeras at >30 days PI.
Means are plotted ± SD. *p < 0.05, **p < 0.01, ***p < 0.001, ****p < 0.0001 (Student's t test). Data are representative of three to four independent experiments with three to five mice per time point.

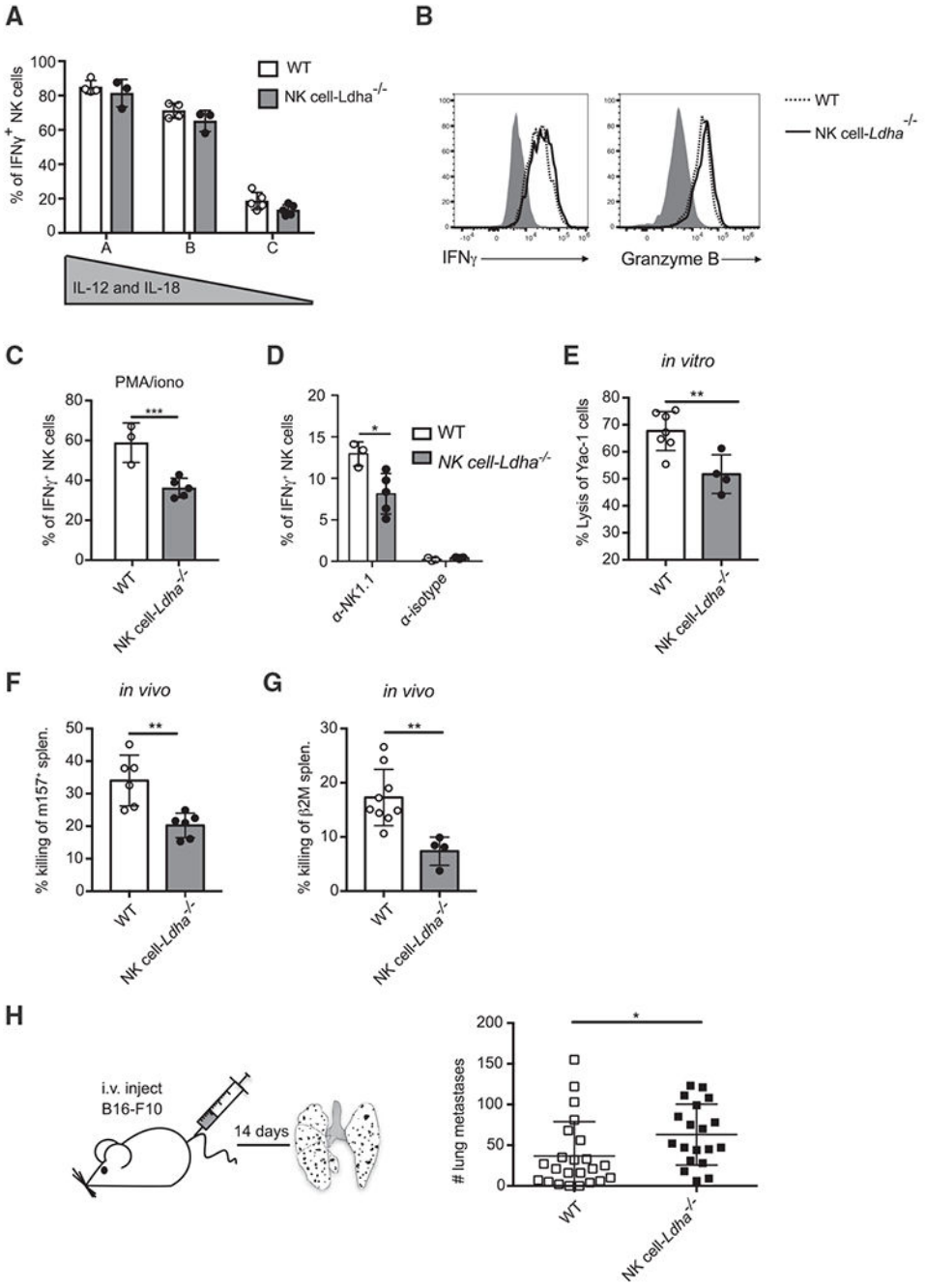

Figure 4. LDHA is required for optimal NK cell effector and anti-tumor function

(A) Percentage of naive $Ldha^{-/-}$ and WT NK cells producing IFN-γ upon *in vitro* stimulation with IL-12 + IL-18 for 5 h (A, 10 ng/mL IL-12 + 20 ng/mL IL-18; B, 1 ng/mL IL-12 + 2 ng/mL IL-18; C, 100 pg/mL IL-12 + 200 pg/mL IL-18).

(B) Representative histograms showing IFN-γ and granzyme B expression in WT (dashed line) and $Ncr1^{Cre} \times Ldha^{flox/flox}$ (solid line) NK cells harvested from mice at day 2 PI.

(C) Graph shows percentage of naive $Ldha^{-/-}$ and WT NK cells producing IFN-γ following *in vitro* stimulation with PMA + ionomycin for 5 h.

(D) Graph shows percentage of naive *Ldha*$^{-/-}$ and WT NK cells producing IFN-γ following *in vitro* stimulation with plate-bound anti-NK1.1 (α-NK1.1) or isotype control antibodies for 5 h.

(E) Lytic killing activity of *Ldha*$^{-/-}$ and WT NK cells incubated at a 20:1 effector/target ratio with calcein-acetoxymethyl-labeled Yac-1 target cells *in vitro* for 5 h.

(F and G) *In vivo* clearance of m157 transgenic (Ly49H ligand-expressing) (F) or β2m KO (MHC class I-deficient) (G) splenocytes 3 and 24 h after intravenous (i.v.) injection, respectively, in NK cell-*Ldha*$^{-/-}$ or WT littermate control mice.

(H) Quantitation of the lung metastases in NK cell *Ldha*$^{-/-}$ or WT littermate control mice challenged i.v. with the B16-F10 melanoma cell line. Results are combined from three independent experiments. *$p < 0.05$ (Mann-Whitney test).

Means are plotted ± SD. (A–G) Data are representative of two to five independent experiments with three to five mice per time point. *$p < 0.05$, **$p < 0.01$, ***$p < 0.001$ (Student’s t test).

KEY RESOURCES TABLE

REAGENT or RESOURCE	SOURCE	IDENTIFIER
Antibodies		
Anti-Mouse CD3ε (clone 17A2)	Tonbo Biosciences	Cat#25-0032; RRID:AB_2621619
Anti-Mouse TCRβ (clone H57-597)	BioLegend	Cat#109220; RRID:AB_893624
CD8α (clone 53-6.7)	BioLegend	Cat#100734; RRID:AB_2075238
NKG2A/C/E (clone 20d5)	BD Biosciences	Cat#740549; RRID:AB_465305
Anti-Mouse NK1.1 (clone PK136)	Tonbo Biosciences	Cat#65-5941; RRID:AB_2621910
Anti-Mouse NKp46 (clone 29A1.4)	BioLegend	Cat#137604; RRID:AB_2235755
Anti-Mouse Ly49H (clone 3D10)	eBioscience/Thermo Fisher	Cat#11-5886-81; RRID:AB_1257160
Anti-Mouse CD45.1 (clone A20)	BioLegend	Cat#110729; RRID:AB_1134170
Anti-Mouse CD45.2 (clone 104)	BioLegend	Cat#109821; RRID:AB_493730
Anti-Mouse CD49b (clone Dx5)	BioLegend	Cat#108918; RRID: AB_2265144
Anti-Mouse/Human CD11b (clone M1/70)	BioLegend	Cat#101223; RRID:AB_755985
Anti-CD27 (clone LG.7F9)	eBioscience/Thermo Fisher	Cat#14-0271-81; RRID:AB_467182
Anti-Mouse KLRG1 (clone 2F1)	Tonbo Biosciences	Cat# 25-5893-82; RRID: AB_1518768
Anti-Mouse Ly49D (clone 4E5)	BioLegend	Cat#138308; RRID:AB_10639939
Ly49G2 (clone 4D11)	eBioscience/Thermo Fisher	Cat #46-5781-82; RRID: AB_1834437
Anti-Mouse Ly49I (clone YLI-90)	BD Biosciences	Cat# 550595; RRID:AB_393770
Anti-Mouse CD69 (clone H1.2F3)	BioLegend	Cat#104524; RRID:AB_2074979
Anti-Human/Mouse Granzyme B (clone GB11)	BioLegend	Cat#515403; RRID:AB_2114575
Anti-Mouse IFN gamma (clone XMG1.2)	Tonbo Biosciences	Cat#20-7311; RRID:AB_2621616
Anti-Mouse CD107a (clone 1D4B)	BioLegend	Cat#121611; RRID:AB_1732051
streptavidin–PE	BioLegend	Cat #405204
streptavidin-APC	BioLegend	Cat #405207
MHC class I monomer D^b/HGIRNASFI (M45)	NIH Tetramer Facility	N/A
MHC class I monomer K^b/SSPPMFRV (M38)	NIH Tetramer Facility	N/A
InVivoMab Anti-Mouse CD8α (NK cell enrichment, clone 2.43)	Bio X Cell	Cat#BE0061; RRID:AB_1125541
InVivoMab Anti-Mouse CD4 (NK cell enrichment, clone GK1.5)	Bio X Cell	Cat#BE0003-1; RRID:AB_1107636
InVivoMab Anti-Mouse CD19 (NK cell enrichment, clone 1D3)	Bio X Cell	Cat#BE0150; RRID:AB_10949187
InVivoMab Anti-Mouse Ter-119 (NK cell enrichment, clone TER-119)	Bio X Cell	Cat#BE0183; RRID:AB_10949625
InVivoMab Anti-Mouse Ly6G (NK cell enrichment, clone 1A8)	Bio X Cell	Cat#BE0075-1; RRID:AB_AB_1107721
InVivoMAb anti-mouse CD3 (NK cell enrichment, clone 17A2)	Bio X Cell	Cat#BE0002; RRID:AB_1107630

REAGENT or RESOURCE	SOURCE	IDENTIFIER
Anti-Mouse NK1.1 (receptor crosslinking clone PK136)	BioLegend	Cat#108758 RRID:AB_2800568
Mouse IgG2a, κ Isotype Ctrl (receptor crosslinking clone MOPC-173)	BioLegend	Cat#400264; RRID:AB_11148947
Purified Rat Anti-Mouse CD16/CD32 (Fc Block clone 2.4G2)	BD Biosciences	Cat#553142; RRID:AB_394657
Bacterial and virus strains		
Murine Cytomegalovirus (MCMV)	J. Sun (PI)	Smith Strain
Chemicals, peptides, and recombinant proteins		
Recombinant Mouse IL-12 Protein	R&D Systems	Cat#419-ML
Recombinant Mouse IL-18	MBL	Cat#B002-5
Recombinant Mouse IL-2 Protein	R&D Systems	Cat#402-ML
Recombinant human IL-15	miltenyi	Cat#130-095-766
Phorbol 12-myristate 13-acetate (PMA)	Sigma-Aldrich	Cat#P8139
Ionomycin calcium salt from *Streptomyces conglobatus* (Ionomycin)	Sigma-Aldrich	Cat#I0634
Critical commercial assays		
BD Cytofix/Cytoperm	BD Biosciences	Cat#554714
Calcein, AM, cell-permeant dye	Thermo Fisher Scientific	Cat#C1430
Seahorse XF Cell Mito Stress Test Kit	Agilent	Cat#103010-100
BioMag Goat Anti-Rat IgG (NK cell enrichment)	QIAGEN	Cat#310107
CellTrace Violet Cell Proliferation Kit	Thermo Fisher Scientific	Cat#C34557
Fixable Viability Dye eFluor 506	eBioscience	Cat#65-0866-18
PicoPure RNA Isolation Kit	Thermo Fisher Scientific	Cat#KIT0214
Deposited data		
Raw Data Files for RNA Sequencing	NCBI Gene Expression Omnibus	GEO: GSE149447
Experimental models: Cell lines		
Yac-1	L. Lanier (PI)	N/A
B16-F10	ATCC	CRL-6475
Experimental models: Organisms/strains		
Mouse: WT or CD45.2: C57BL/6J	The Jackson Laboratory	Stock#000644; RRID:IMSR_JAX:000664
Mouse: WT or CD45.1: B6.SJL-*Ptprc*^{a} *Pepc*^{b}/BoyJ	The Jackson Laboratory	Stock#002014; RRID:IMSR_JAX:002014
Mouse: CD45.1xCD45.2	J. Sun (PI)	N/A
Mouse: *Ldha*^{flox}	M. Li (PI)	N/A
Mouse: β2 m KO	The Jackson Laboratory	Stock#002087; RRID:IMSR_JAX:002087
Mouse: *Ncr1*^{iCre}	E. Vivier (PI) (Narni-Mancinelli et al., 2011)	N/A
Mouse: m157 transgenic	W. Yokoyama (PI) (Tripathy et al., 2008)	N/A
Mouse: *CD4*^{Cre}	The Jackson Laboratory	Stock#022071; RRID:IMSR_JAX:022071

REAGENT or RESOURCE	SOURCE	IDENTIFIER
Mouse: Vav^{Cre}	The Jackson Laboratory	Stock#008610; RRID:IMSR_JAX:008610;
Mouse: $Klra8^{-/-}$ or Ly49H-deficient	S. Vidal (PI) (Fodil-Cornu et al., 2008)	N/A
Oligonucleotides		
TaqMan *Ldha* Mm01612132_g1	Thermo Fisher Scientific	Cat#4331182
TaqMan *Actb* Mm02619580_g1	Thermo Fisher Scientific	Cat#4331182
Software and algorithms		
DESeq2 (v.1.22.2)	Love et al., 2014	http://bioconductor.org/packages/release/bioc/html/DESeq2.html
Trimmomatic (v.0.36)	Bolger et al., 2014	http://www.usadellab.org/cms/?page=trimmomatic
Bowtie2 (v.2.3.4)	Langmead and Salzberg, 2012	http://bowtie-bio.sourceforge.net/bowtie2/index.shtml
Salmon (v.0.13.1)	Patro et al., 2017	https://salmon.readthedocs.io/en/latest/salmon.html
tximport (v.1.10.1)	Soneson et al., 2015	https://bioconductor.org/packages/release/bioc/html/tximport.html
goseq (v.1.34.1)	Young et al., 2010	https://bioconductor.org/packages/release/bioc/html/goseq.html
KEGG.db (v.3.2.3)	Bioconductor	https://bioconductor.org/packages/release/data/annotation/html/KEGG.db.html
PANTHER.db (v.1.0.4)	https://bioconductor.org/packages/release/data/annotation/html/PANTHER.db.html	https://bioconductor.org/packages/release/data/annotation/html/PANTHER.db.html
R (v.3.5.1)	https://www.r-project.org/	https://www.r-project.org/
UCSC mm10 Known Gene Annotation Package (v.9)	Bioconductor	https://bioconductor.org/packages/release/data/annotation/html/TxDb.Mmusculus.UCSC.mm10.knownGene.html